High efficiency Cu_2ZnSnS_4 solar cells over FTO substrate and its CZTS/CdS interface passivation via thermal evaporated Al_2O_3

Esteban Ojeda-Durán,*[a] Karim Monfil-Leyva,[a] Jacob Andrade-Arvizu,[b] Ignacio Becerril-Romero,[b] Yudania Sánchez,[b] Robert Fonoll-Rubio,[b] Maxim Guc,[b] Zacharie Jehl Li-Kao,[c] José A. Luna-López,[a] Edgardo Saucedo.[c]

Abstract. Fabrication on SLG/FTO transparent substrates gives an important advance to fabrication of tandem solar cells. In addition, a possible passivation using Al2O3 which can be deposited with cheap systems can opens an increase in development of CZTS solar cells. In this work, we report the simultaneous use of FTO/Mo(20nm) as a transparent substrate and Al2O3 as passivation layer at the pn interface CZTS solar cells. The best devices showed efficiencies of 7.7% (Voc=677 mV) and, 7.3% (Voc=700 mV). A complete morphological, structural and electrical analysis is discussed.

Introduction

Kesterite materials (Cu_2ZnSnS_4, $Cu_2ZnSnSe_4$, and $Cu_2ZnSn(S,Se)_4$) are a promising class of thin film photovoltaic absorbers, containing exclusively earth-abundant and low toxicity elements such as Cu, Sn, Zn, Se, and S [1]. One of its properties is the tunability of the bandgap of kesterite, up to 1.5 eV for the pure sulfur compound Cu_2ZnSnS_4 (CZTS), which makes it suitable for tandem solar cells application [2]. Tandem devices involving CZTS have been reported: Hajijafarassar *et al.* [3] reported a complete tandem solar cell using Si (type n) and CZTS showing an efficiency of 1.1% and Valentini *et al.* [4] reported a tandem solar cell using Si (type p) and CZTS showing 3.5% in efficiency. The use of a transparent contact, often a transparent conductive oxide (TCO) as back contact, is critical in that context, and recently Jeong Shin *et al.* [5] demonstrated the feasibility of such contact on $Cu(In,Ga)Se_2$ solar cells. The similarities between chalcopyrite and kesterite allows for a direct transfer of ideas and concepts, with possible refinements specific for each technology. Recently, Espindola-Rodriguez *et al.* [6] fabricated CZTSSe solar cells using FTO as back contact with a very thin-layer of molybdenum (Mo) (20 nm), promoting the formation of an $MoSe_2$ interfacial layer improving the contact's ohmicity, and leading to efficiencies of η=6.3% (front illumination) and, η=7.7% (bifacial illumination) [6]. The direct comparison of the ITO and FTO layers shows that the former could limit the performance of the solar cells due to a possible diffusion of indium atoms through the absorber layer, and, as a consequence, a degradation of the electrical conductivity of ITO [7-9]. On the other hand, FTO showed a high stability up to 500°C before slightly degrading at higher temperatures [10,11]. Mainly, the FTO degradation is ascribed to the diffusion of fluorine atoms to the absorber film, which can be avoided, by adding a molybdenum layer as diffusion barrier, while the Mo reaction with sulfur forms MoS_2 [6,11,12]. Additionally, an ultrathin MoS_2 layer is known to improve the contact ohmicity and often deemed necessary in high efficiency devices [13].

On the other hand, reducing the V_{oc} deficit is currently the most important challenge faced by the kesterite community, and the perspective of wide bandgap top cell application in tandem devices makes this issue even more critical. Avoiding interface recombination (specifically, MoS_2/CZTS and CZTS/CdS) is a key strategy in that context. For instance, for the MoS_2/CZTS interface, Yan *et al.* [14] reported the use of Al_2O_3 to limit the growth of MoS_2, obtaining an efficiency of 11%. In the case of the CZTS/CdS interface, Sun *et al.* [15] reported a V_{oc} of 657 mV using an Al_2O_3 thin film deposited by Atomic Layer Deposition (ALD). The use of H_2O vapor and Trimethyl-aluminium (TMA) in Al_2O_3 deposition by ALD questions whether hydrogen is the main passivation factor, rather than the Al_2O_3 layer. On the other hand, H. Xie *et al.* [16] investigated the chemical deposition of an ultrathin $Al(OH)_3$ layer to passivate the surface of the CZTSSe. Xie *et al.* observed a reduction in the recombination at the CZTSSe/CdS interface, with an improvement in the shunt resistance. The authors also demonstrated an epitaxial relationship of $Al(OH)_3$ with kesterite and CdS, corroborating an effective interface passivation with this chemical approach.

In this work, we aim at simultaneously optimizing the front and back interface and study the effect of a passivating Al_2O_3 layer deposited by thermal evaporation in CZTS/CdS interface for devices fabricated on transparent substrates.

The deposition of Al_2O_3 by thermal evaporation avoids an extra chemical process (as was reported by Sun *et al.* [15] and Xie *et al.* [16]) and, as consequence, a possibly modification in composition and structure. All devices with thermally evaporated Al_2O_3 showed an increased V_{oc} but a slightly decreased fill factor (FF), suggesting an increase in the series resistance at the CZTS/Al_2O_3/CdS interfaces. Promising record efficiencies of 7.7% (677 mV) and 7.3% (700 mV) are obtained for CZTS solar cell (without Al_2O_3 passivation) and CZTS solar cell (with Al_2O_3 passivation), respectively. Such voltages are among the highest reported so far for this class of materials, even more so as the devices reported in this study use a transparent FTO substrate. A proof of concept for sulfur kesterite solar cells to be used in tandem devices is thus deemed possible if both, the front and back interface are simultaneously optimized.

Experimental details

Substrates preparation (FTO and soda lime glass). CZTS thin films were grown onto commercial FTO coated (800 nm and sheet resistance <10 Ω/□) soda lime glass (SLG) substrates and SLG substrates by a sequential process within the same batch. The SLG substrates were used for the characterization of kesterite films exclusively. FTO and SLG substrates were cleaned with isopropanol

and then with deionized water in ultrasonic bath during 10 minutes in both cases. Immediately, after the cleaning process, 20 nm of Molybdenum (Mo) was deposited by DC magnetron sputtering (Alliance Concept CT100) on the FTO substrates.

Precursor synthesis. The stacked metallic films were deposited by DC magnetron sputtering (Alliance Concept 450) where Cu, Sn and Zn elemental targets were used. The stacked metallic films were deposited at the same time in both FTO and SLG substrates to favour reproducibility between the samples. These depositions were optimized to produce Cu-poor and Zn-rich CZT precursor materials as it has been reported elsewhere [17]. The cationic ratios are Cu/(Zn+Sn)= 0.7, 0.76 and, 0.73 & Zn/Sn= 1.0, 1.1, and 1.2, labelled as samples A, B, and C, respectively (Table SI, Electronic Supplementary Information). The cationic ratios were determined by X-ray fluorescence (Fisherscope XVD) on a reference sample without FTO (SLG substrate). The complete detailed metallic deposition and sulfurization process are described in Electronic Supplementary Information. After deposition, the CZT precursors were simultaneously sulfurized inside of a graphite box containing sulfur (100 mg) and tin (50 mg) powders, using a tubular furnace and the following two-step annealing: 15 min at 250°C (1 mbar Ar flux) and 30 min at 570°C (1 bar total Ar pressure) (Fig S1, Electronic Supplementary Information). The thickness of the absorbers is ~1.4 µm as measured by X-ray fluorescence.

Solar cells fabrication (without and with Al_2O_3). Prior to the Al_2O_3 deposition, the samples on FTO substrate were etched using a KCN solution (2% w/V, 2 min) [18]. A ~3 nm Al_2O_3 layer was deposited by thermal evaporation (Univex 250) in some of the samples. The deposition by thermal evaporation was justified to avoid the use of hydrogen in Al_2O_3 deposition (commonly used in Al_2O_3 deposited by atomic layer deposition [13, 19-21]). Then, a 50 nm thick CdS buffer layer was deposited by chemical bath deposition. Finally, the devices on FTO substrate were completed with i-ZnO (50 nm)/ITO (200 nm) layers deposited by DC magnetron sputtering (Alliance Concept CT100). In this way, two different architectures were studied: SLG/FTO/Mo(20nm)/CZTS/CdS/i-ZnO/ITO and SLG/FTO/Mo(20nm)/CZTS/Al_2O_3/CdS/i-ZnO/ITO as shown in Fig. S2 (Electronic Supplementary Information). Individual 9 mm^2 solar cells were isolated using a manual microdiamond scriber (OEG MR200) and characterized by means of J-V illuminated curves (AM 1.5) and external quantum efficiency (EQE). Neither antireflective coating (ARC) nor metallic grids were used on the solar cells. The solar cells over FTO are labelled as follow: solar cells ANA, BNA, and CNA (samples A, B, and C, respectively) without Al_2O_3, and solar cells AWA, BWA, and CWA (samples A, B, and C, respectively) with ~3 nm of Al_2O_3.

CZTS films and CZTS solar cells characterization. The as-grown CZTS-solar cells (FTO substrate) were analysed by Raman spectroscopy using a Horiba Jobin-Yvon FHR640 spectrometer coupled with CCD camera and excited by a diode-pumped solid-state laser of 532 nm and He-Cd gas laser (325 nm). J-V curves were measured under light conditions using a Sun 3000 class AAA Abet Technologies solar simulator (1 sun illumination). 1 sun illumination was achieved with a 1kW lamp over a 210 x 210 mm field. The EQE measurements were obtained using a Bentham PVE3000 system calibrated with Si and Ge photodiodes. EQE measurements were excited with 75W Xenon and 100W Quartz halogen (QTH). The monochromator configuration was set with triple grating, symmetric, single Czerny-Turner, 300 mm focal length. Top and cross section SEM images from the CZTS film and the solar cell structure were taken using a Zeiss Series Auriga microscope using 5 kV as acceleration voltage. Zeiss Series Auriga is equipment with a Schottky Field Emitter as source. The analysis in this communication will be focused on samples B (BNA and BWA). Otherwise, a complete analysis from the bare kesterite films and solar cells samples is presented in the Electronic Supplementary Information document.

Results and discussion

In Fig. S3 (Electronic Supplementary Information) is shown the Raman spectra with an excitation of 532 nm. Only the peaks related to CZTS compound were detected [22], while the low width of the main peak indicated a high crystalline quality of the sample [22]. In the inset figure is shown the Raman spectra with an excitation of 325 nm. All the samples showed traces of ZnS associated to the presence of this compound in CZTS films. In Fig. S4 (Electronic Supplementary Information) are shown the top-view SEM images. The samples showed big grains with average grain sizes of 1.5 µm (Sample A), 1.3 µm (Sample B), and 1.6 µm (Sample C), respectively. Sample A (Fig. S4a, Electronic Supplementary Information) is showing some voids in the surface. Sample C (Fig. S4c, Supplementary Information) is showing a compact morphology. Finally, Sample B (Fig. S4b, Supplementary Information) is showing less compact morphology than Sample C. Likewise, the shunt paths can be avoided with the help of an Al_2O_3 layer acting as insulating layer.

After Raman and SEM analysis, CZTS solar cells were optoelectronically characterized. In Fig. 1 are shown the J-V illuminated curves from BNA & BWA solar cells. The sample BNA showed the following parameters: η=7.7%, V_{oc}=677 mV, J_{sc}=17.8 mA/cm^2, and FF=63.8%, whereas the sample BWA showed the parameters η=7.3%, V_{oc}=700 mV, J_{sc}=18.2 mA/cm^2, and FF=57%. To the best of our knowledge, the efficiencies of 7.7% and 7.3% are close to the highest reported in kesterite solar cells using a TCO substrate, particularly for a sulfur kesterite material [6-8,23]. In Fig. S5 (Electronic Supplementary Information) are shown the box-plot diagrams from complete solar cells BNA and BWA (10 cells in each sample). The importance of Al_2O_3 as passivation layer is shown in sample BWA which showed less disperse values in V_{oc} and efficiency, indicating that the interface passivation significantly improves the reproducibility. In J_{sc}, the box plot in BWA showed an increment; unfortunately, FF decreases as Al_2O_3 layer was deposited. Finally, the efficiency values in BWA are from 6.3% to 7.3%. Fig. S6 (Electronic Supplementary Information) are shown the J-V illuminated curves from CZTS solar cells without Al_2O_3 (Fig. S6a) and with Al_2O_3 passivation layer (Fig. S6b). With the figures of merit from all the samples, the Al_2O_3 passivation layer demonstrates a limited but a clear beneficial influence on the V_{oc}. The peak efficiency value was however slightly lower due to the FF degradation. The electrical parameters from solar cells without Al_2O_3 and with Al_2O_3 were extracted from dark J-V curves fitting [24, 25]: shunt resistance (R_{sh}), series resistance (R_s), ideality factor (A), and reverse saturation current density (J_0). A summary of the optoelectronic properties of BNA and BWA devices is shown in

Table I. The complete summary of all the samples is shown in Table SI (Electronic Supplementary Information). R_{sh} values were obtained from G_{sh} curves (Fig.S7, Supporting Information). The value in R_{sh} from BNA sample is 9,091 Ω/cm^2. This shunt resistance value benefits in the efficiency of 7.7% obtained. On the other hand, sample BWA showed a shunt resistance of 5,555.6 Ω/cm^2, therefore, they showed a very good efficiency (7.3%). The decrease in R_{sh} could be to the major formation of voids in Mo/CZTS interface (as are shown in Fig.2) and secondary phases, due to the wettability behaviour between the substrate and metal precursor [26, 27]. In the same way, these voids could be formed by liquid phase formation due to compositional nonuniformity during the annealing process, compositional mismatch of the metal precursor itself, and Zn volatilization during the process when using metal precursors [28]. R_s curves are shown in Fig.S8 (Electronic Supplementary Information). Series resistances from samples BNA (6.0 Ω·cm^2) and BWA (6.8 Ω·cm^2) are quite similar. While the voltage is marginally improved by the introduction of an Al_2O_3 passivation layer, the degradation of the FF is ascribed to an increase in the series resistance at the interface; hence, it is possible that despite being only 3 nm thick, this layer acts as a barrier hindering the transport of photoelectrons. Thus, even thinner passivation layers may have to be considered in future experiments to reach a perfect balance between limited series resistance and passivation effect. In that regard, the ideality factor (A) was calculated from Fig. S8 (Electronic Supplementary Information).

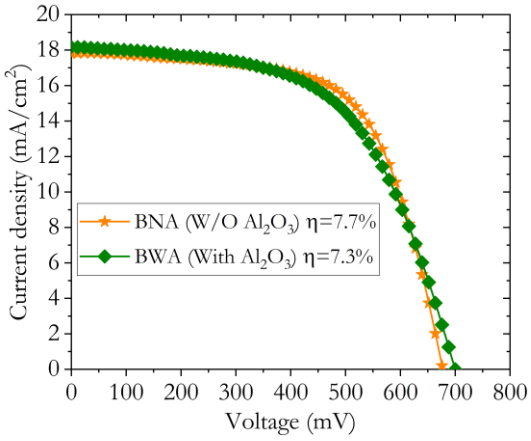

Fig. 1. J-V curves from CZTS solar cell a) without Al_2O_3 (BNA) and b) with Al_2O_3 (BWA).

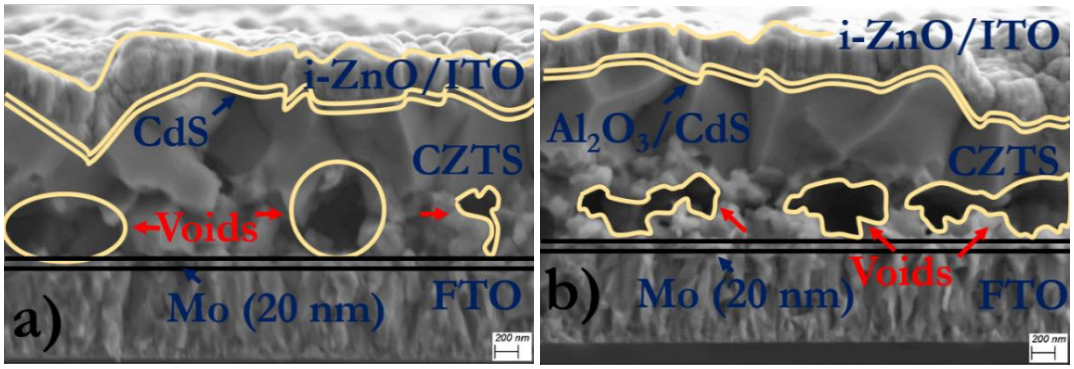

Fig. 2. SEM Cross Section-view from the samples a) BNA and, b) BWA.

Table I. Optoelectronic properties of devices without Al_2O_3 (BNA) and with Al_2O_3 (BWA) onto FTO substrate.

Sample	J_{sc} (mA/cm^2)	V_{oc} (mV)	FF (%)	η (%)	R_s (Ω·cm^2)	R_{sh} (Ω·cm^2)	A	J_0 (mA/cm^2)	$V_{oc(SQ)}$ deficit (mV)	Eg (eV)
BNA	17.8	677	63.8	7.7	6.0	9091.0	1.7	2.8×10^{-3}	561	1.50
BWA	18.2	700	57	7.3	6.8	5555.6	1.8	2.6×10^{-3}	523	1.50

The samples BNA and BWA showed similar values: 1.7 and 1.8, respectively. These values demonstrate very good junction quality. Furthermore, ideality factor values showed that the recombination current is the dominant charge transport mechanism [29]. In the same way, the J_0 was calculated from the same J-V dark curves (Fig. S9, Electronic Supplementary Information). There is no big difference in J_0 between the samples BNA (2.8×10^{-3} mA/cm^2) and BWA (2.6×10^{-3} mA/cm^2), indicating relatively similar recombination processes [30]. In the same Table I, the $V_{oc(SQ)}$ deficit is shown. The V_{oc} deficit is calculated by comparing the device's voltage with the $V_{oc(SQ)}$, which is the maximum thermodynamic V_{oc} achievable for a given bandgap [1]. This parameter was calculated with respect to the maximum theoretic value represented by the Shockley-Queisser limit [31,32]. The smallest $V_{oc(SQ)}$ deficit is obtained for the sample BWA which has 523 mV; sample BNA shows a $V_{oc(SQ)}$ deficit of 561 mV. The $V_{oc(SQ)}$ value of sample BWA significantly increased, which gives the opportunity to a future improvement with the use of Al_2O_3. The 523 mV in $V_{oc(SQ)}$

deficit in the sample with FTO substrate and Al_2O_3 passivation layer is close comparing with previously published results on record CZTS-based solar cells, using the well stablished Mo as substrate and without passivation layer (501 mV [13], 503 mV [33], 495 mV [34]).

On the other hand, the external quantum efficiencies (EQE) and J_{sc} integrated from BNA and BWA samples are shown in Fig. S10 (Electronic Supplementary Information). Sample BWA (Fig. S10a) showed good response on the 500-600 nm region but a lower response in the CZTS region (550-850 nm). Additionally, the increase in response in 500-600 nm region could be related to a slightly thinner CdS buffer layer. The growth rate of CdS on Al_2O_3 could be lower than that growth on CZTS absorber, despite CdS buffer layer was deposited in the same batch [15]. In the same way, BWA is showing a decrease in response in the CZTS region (550-850 nm). This fact could be attributed to destructive interferences in that spectral region [35], and the addition of an antireflection coating would probably even the EQEs in that spectral range. The EQE measurements from all the samples are shown in Fig. S11 (Electronic Supplementary Information). The samples with Al_2O_3 layer showed a slightly increment in 500-600 range. Finally, from the EQE we can obtain the bandgap using the inflection of the dEQE/dλ curves. The Eg values are shown in Table I [36].

In summary, we report on the fabrication of CZTS solar cells on transparent FTO substrate with the presence of an Al_2O_3 passivation layer. An improvement of the voltage is observed, which is consistent with a passivation of interface defects; however, the series resistance is slightly increased leading to a degradation of the fill factor. As a result, a slightly lower efficiency is obtained, which indicates that a thinner passivation layer ought to be used to obtain an optimal interface combining low series resistance and interface defect passivation. Nevertheless, efficiencies are obtained with values around 7.5%, and a voltage of 700 mV. The feasibility of sulfur kesterite absorbers on transparent substrate is demonstrated, but additional efforts are necessary to optimize the front interface.

Conflicts of interest

There are no conflicts to declare.

Acknowledgements

This research was supported by the H2020 Programme under the project INFINITE-CELL (H2020-MSCA-RISE-2017-777968), by the Spanish Ministry of Science, Innovation and Universities under the IGNITE project (ENE2017-87671-C3-1-R), and by the European Regional Development Funds (ERDF, FEDER Programa Competitivitat de Catalunya 2007-2013). Authors from IREC and the University of Barcelona belong to the SEMS (Solar Energy Materials and Systems) Consolidated Research Group of the "Generalitat de Catalunya" (Ref. 2017 SGR 862). M.P. thanks the Government of Spain for the Ramon y Cajal Fellowship (RYC-2017-23758). This research was also supported by Consejo Nacional de Ciencia y Tecnología (CONACYT) with the scholarship No. 433146 and with the project CB-CONACYT-255062. Finally, this research was also supported by Programa de Fortalecimiento de la Calidad Educativa (PFCE 2019) and by Project VIEP 2019.

Notes and references

1 S. Giraldo, Z. Jehl, M. Placidi, V. Izquierdo-Roca, A. Pérez-Rodríguez, E. Saucedo. "Progress and Perspectives of Thin Film Kesterite Photovoltaic Technology: A Critical Review". Adv. Mater. 2019, 31, 1806692. DOI: 10.1002/adma.201806692.

2 Alexis De Vos. "Detailed balance limit of the efficiency of tandem solar cells" J. Phys. D: Appl. Phys., 13 (1980) 839-46. DOI: http://iopscience.iop.org/0022-3727/13/5/018.

3 A. Hajijafarassar, F. Martinho, F. Stulen, S. Grini, S. López-Mariño, M. Espíndola-Rodríguez, M. Döbeli, S. Canulescu, E. Stamate, M. Gansukh, S. Engberg, A. Crovetto, L. Vines, J. Schou, O. Hansen. "Monolithin thin-film chalcogenide-silicon tandem solar cells enabled by a diffusion barrier". Sol. Energy Mater. Sol. Cells 207 (2020) 110334. DOI: https://doi.org/10.1016/j.solmat.2019.110334.

4 M. Valentini, C. Malerba, L. Serenelli, M. Izzi, E. Salza, M. Tucci, A. Mittiga. "Fabrication of monolithic CZTS/Si tándem cells by development of the intermediate connection". Solar Energy 190 (2019) 414-419. DOI: https://doi.org/10.1016/j.solener.2019.08.029.

5 Min Jeong Shin, Sungeun Park, Ahreum Lee, Se Jun Park, Ara Cho, Kihwan Kim, Seung Kyu Ahn, Joo Hyung Park, Jinsu Yoo, Donghyeop Shin, Inyoung Jeong, Jae Ho Yun, Jihye Gwak, Jun-Sik Cho. "Bifacial photovoltaic performance of semitransparent ultrathin Cu(In,Ga)Se2 solar cells with front and rear transparent conducting oxide contacts". Applied Surface Science. 535 (2021) 147732.

6 M. Espindola-Rodriguez, D. Sylla, Y. Sánchez, F. Oliva, S. Grini, M. Neuschitzer, L. Vines, V. Izquierdo-Roca, E. Saucedo, M. Placidi. "Bifacial kesterite solar cells on FTO substrates". ACS Sustainable Chem. Eng. 2017, 5, 11516-11524. DOI: 10.1021/acssuschemeng.7b02797.

7 J. Ge, J. Chu, J. Jiang, Y. Yan, P. Yang. "The interfacial reaction at ITO back contact in kesterite CZTSSe bifacial solar cells". ACS Sustainable Chem. Eng. 2015, 3, 3043-3052. DOI: 10.1021/acssuschemeng.5b00962.

8 J. Ge, J. Chu, J. Jiang, Y. Yan, P. Yang. "Characteristics of In-substituted CZTS thin film and bifacial solar cell". ACS Appl. Mater. Interfaces 2014, 6, 21118-21130. DOI: 10.1021/am505980n.

9 Jung-Sik Kim, Jin-Kyu Kang, Dae-Kue Hwang. "High efficiency bifacial Cu2ZnSnSe4 thin-film solar cells on transparent conducting oxide glass substrates". APL. Materials. 4, 096101 (2016). DOI: https://doi.org/10.1063/1.4962145.

10 I. Becerril-Romero, D. Sylla, M. Placidi, Y. Sánchez, J. Andrade-Arvizu, V. Izquierdo-Roca, M. Guc, A. Pérez-Rodríguez, S. Grini, L. Vines, B. Pusay, R. Almache, J. Puigdollers, P. Pistor, E. Saucedo, M. Espíndola-Rodríguez. "Transition-metal oxides for kesterite

solar cells developed on transparent substrates". ACS Appl. Mater. Interfaces. 2020, 12, 30, 33656-33669. DOI: 10.1021/acsami.0c06992.

11 M. Ould Salem, R. Fonoll, S. Giraldo, Y. Sánchez, M. Placidi, V. Izquierdo-Roca, C. Malerba, M. Valentini, D. Sylla, A. Thomere, D. Ould Ahmedou, E. Saucedo, A. Pérez-Rodríguez, Z. J. Li-Kao. "Over 10% Efficient wide bandgap CIGSe solar cells on transparent substrate with Na predeposition treatment". Sol. RRL 2020, 2000284. DOI: 10.1002/solr.202000284.

12 J. J. Scragg, J. Timo Wätjen, Marika Edoff, Tove Ericson, Tomas Kubart, Charlotte Platzer-Björkman. "A detrimental reaction at the molybdenum back contact in Cu2ZnSn(S,Se)4 thin-film solar cell". J. Am. Chem. Soc. 2012, 134, 19330-19333. DOI: 10.1021/ja308862n.

13 C. Platzer-Björkman, N. Barreau, M. Bär, L. Choubrac, L. Grenet, J. Heo, T. Kubart, A. Mittiga, Y. Sánchez, J. Scragg. "Back and front contacts in kesterite solar cells: state-of-the-art and open questions. J. Phys. Energy 1 044005 (2019). DOI: 10.1088/2515-7655/ab3708.

14 C. Yan J. Huang, K. Sun, S. Johnston, Y. Zhang, H. Sun, A. Pu, M. He, F. Liu, K. Eder, L. Yang, J.M. Cairney, N.J. Ekins-Daukes, Z. Hameiri, J.A. Stride, S. Chen, M.A. Green, X. Hao. "Cu2ZnSnS4 solar cells with over 10% power conversion efficiency enabled by heterojunction heat treatment". Nature energy. 3, 764-772 (2018). DOI: 10.1038/s41560-018-0206-0.

15 Sun, H., Sun, K., Huang, J., Yan, C., Liu, F., Park, J., Pu, A., Stride, J.A., Green, M.A., Hao, X. Efficiency enhancement of kesterite Cu2ZnSnS4 solar cells via solution processed ultrathin tin oxide intermediate layer at absorber/buffer interface. ACS Appl. Energy Mater. 1, 2018 154–160. https://doi.org/10.1021/acsaem.7b00044.

16 H. Xie, Y. Sánchez, P. Tang, M. Espíndola-Rodríguez, M. Guc, L. Calvo-Barrio, S. López-Marino, Y. Liu, J. R. Morante, A. Cabot, V. Izquierdo-Roca, J. Arbiol, A. Pérez-Rodríguez, E. Saucedo. "Enhanced hetero-junction quality and performance of kesterite solar cells by Aluminum Hydroxide nanolayers and efficiency limitation revealed by Atomic-resolution scanning transmission electron microscopy". Sol. RRL 2019, 3, 1800279. DOI: 10.1002/solr.201800279.

17 S. van Duren, D. Sylla, A. Fairbrother, Y. Sánchez, S. López-Marino, J. A. Márquez Prieto, V. Izquierdo-Roca, E. Saucedo, T. Unold. "Pre-annealing of metal stack precursors and its beneficial effect on kesterite absorber properties and device performance". Sol. Energy Mater. Sol. Cells 2018, 185, 226-232. DOI: 10.1016/j.solmat.2018.04.022.

18 A. Fairbrother, E. García-Hemme, V. Izquierdo-Roca, X. Fontané, F.A. Pulgarín-Agudelo, O. Vigil-Galán, A. Pérez-Rodríguez, E. Saucedo. "Development of a selective chemical etch to improve the conversion efficiency of Zn-rich Cu2ZnSnS4 solar cells". J. Am. Chem. Soc. Vol. 134, 8018-8021, 2012. DOI: 10.1021/ja301373e.

19 J. Park, J. Huang, J. Yun, F. Liu, Z. Ouyang, H. Sun, C. Yan, K. Sun, K. Kim, J. Seidel, S. Chen, M.A. Green, X. Hao. "The role of hydrogen from ALD-Al2O3 in kesterite Cu2ZnSnS4 solar cells: grain surface passivation." Adv. Energy Mater. 1701940, 1-7, 2018. DOI: 10.1002/aenm.201701940.

20 M. E. Erkan, V. Chawla, M. A. Scarpulla. "Reduced defect density at the CZTSSe/CdS interface by atomic layer deposition of Al2O3". J. Appl. Phys. 2016, 119, 194504. DOI:10.1063/1.4948947.

21 Y. S. Lee. T. Gershon, T. K. Todorov, W. Wang, M. T. Winkler, M. Hopstaken, O. Gunawan, J. Kim. "Atomic Layer Deposited Aluminum Oxide for Interface Passivation of Cu2ZnSn(S,Se)4 Thin-Film Solar Cells". Adv. Energy Mater. 2016, 6, 1600198. DOI: 10.1002/aenm.201600198.

22 M. Guc, S. Levcenko, I. V. Bodnar, V. Izquierdo-Roca, X. Fontane, L. V. Volkova, E. Arushanov, A. Pérez-Rodríguez. "Polarized Raman scattering study of kesterite type Cu2ZnSnS4 single crystals". Sci. Rep. Vol. 6, 19414, 2016. DOI:10.1038/srep19414.

23 J. Ge, J. Chu, Y. Yan, J. Jiang, P. Yang. "Co-electroplated kesterite bifacial thin-film solar cells: A study of sulfurization temperature". ACS Appl. Mater. Interfaces 2015, 7, 10414-10428. DOI: 10.1021/acsami.5b01641.

24 J. R. Sites, P. H. Mauk, "Diode quality factor determination for thin-film solar cells". Solar cells, 27 (1989) 411-417. https://doi.org/10.1016/0379-6787(89)90050-1.

25 S. S. Hegedus, W. N. Shafarman, "Thin-film solar cells: device measurements and analysis". Prog. Photovolt: Res. Appl. 2004; 12: 155-176. DOI: 10.1002/pip.518.

26 Se-Yun Kim, Seung-Hyun Kim, Sanghun Hong, Dae-Ho Son, Young-Ill Kim, Sammi Kim, Kwangseok Ahn, Kee-Jong Yang, Dae-Hwan Kim, and Jin-Kyu Kang. "Secondary phase formation mechanism in the Mo-back contact region during sulfo-selenization using a metal precursor: effect of wettability between a liquid metal and substrate on secondary phase formation". ACS Appl. Mater. Interfaces 2019, 11, 23160-23167. DOI: 10.1021/acsami.9b03969.

27 S. Giraldo, R. Fonoll-Rubio, Z. J. Li-Kao, Y. Sánchez, L. Calvo-Barrio, V. Izquierdo-Roca, A. Pérez-Rodríguez, E. Saucedo. "Rear interface engineering of kesterite Cu2ZnSnSe4 solar cells by adding CuGaSe2 thin layers". Prog. Photovolt. Res. Appl. 2020; 1-10. DOI: 10.1002/pip.3366.

28 Se-Yun Kim, Dae-Ho Son, Seung-Hyun Kim, Young-Ill Kim, Sammi Kim, Kwangseok Ahn, Kee-Jeong Yang, Jin-Kyu Kang, and Dae-Hwan Kim. "Effect of Cu-Sn-Se Liquid Phase on Grain Growth and Efficiency of CZTSSe Solar Cells" Adv. Energy Mater. 2020, 1903173. DOI: 10.1002/aenm.201903173.

29 S. S. Mali, P. S. Shinde, C. A. Betty, P. N. Bhosale, Y. W. Oh, P. S. Patil. "Synthesis and characterization of Cu2ZnSnS4 thin films by SILAR method". J. Phys. Chem. Solids. 73 (2012) 735-740. DOI: https://doi.org/10.1016/j.jpcs.2012.01.008.

30 Cuevas Andres. "The recombination parameter J0". Energy Procedia 55 (2014) 53-62. DOI: https://doi.org/10.1016/j.egypro.2014.08.073

31 W. Shockley, H. Queisser. "Detailed balance limit of efficiency of p-n junction solar cells". J. of Appl. Phys. 32, 510 (1961). DOI: 10.1063/1.1736034.

32 F. Meillaud, A. Shah, C. Droz, E. Vallat-Sauvain. C. Miazza. "Efficiency limits for single-junction and tandem solar cells". Sol. Energy Mater. Sol. Cells 90 (2006) 2952-2959. DOI: 10.1016/j.solmat.2006.06.002.

33 S. Bourdais, C. Choné, B. Delatouche, A. Jacob, G. Larramona, C. Moisan, A. Lafond, F. Donatini, G. Rey, S. Siebentritt, A. Walsh, G. Dennler. "Is the Cu/Zn disorder the main culprit for the voltage deficit in kesterite solar cells?" Adv. Energy Mater. 2016, 6, 1502276. DOI: 10.1002/aenm.201502276.

34 Se-Yun Kim, Dae-Ho Son, Seung-Hyun Kim, Young-Ill Kim, Sammi Kim, Kwangseok Ahn, Kee-Jeong Yang, Jin-Kyu Kang, and Dae-Hwan Kim. “Effect of Cu-Sn-Se Liquid Phase on Grain Growth and Efficiency of CZTSSe Solar Cells” Adv. Energy Mater. 2020, 1903173. DOI: 10.1002/aenm.201903173.
35 X. Cui, K. Sun, J. Huang, C.-Y. Lee, C. Yan, H. Sun, Y. Zhang, F. Liu, M. A. Hossain, Y. Zakaria, L. H. Wong, M. Green, B. Hoex, X. Hao. “Enhanced heterojunction interface quality to achieve 9.3% efficient Cd-free Cu2ZnSnS4 solar cells using atomic layer deposition ZnSnO buffer layer”. Chem. Mater. 2018, 30, 7860-7871. DOI: 10.1021/acs.chemmater.8b03398.
36 T. Gokmen, O. Gunawan, T. K. Todorov, D. Mitzi. “Band tailing and efficiency limitation in kesterite solar cells”. *Appl. Phys. Lett.* 103, 103506 (2013). DOI: https://doi.org/10.1063/1.4820250.